J. Fluid Mech. (1992), *vol.* 245, *pp.* 701–722

Close interaction between a vortex filament and a rigid sphere

By GIANNI PEDRIZZETTI

Dipartimento di Ingegneria Civile, Università di Firenze, via S. Marta 3, 50139 Firenze, Italy

(Received 7 November 1991 and in revised form 7 May 1992)

The evolution of a linear vortex filament close to a rigid sphere is investigated at high Reynolds number. The limiting evolution in an ideal flow, is analysed using a cutoff method and the results are compared with those of a singular vortex approach able to account for a viscous effect on the vortex structure evolution. The computed results show the creation of a closed vortex structure in ideal flow and also, at low Reynolds number, an unrealistic reattachment of the vortex to the surface of the body. The nature of the boundary-layer development, when the no-slip condition is satisfied, is calculated near the symmetry plane. The solutions show the development of an unsteady, vortex-driven, separating boundary layer with the three-dimensional separations dependent on the initial distance of the filament from the wall. All the solutions ultimately show a rapid growth of the secondary vorticity field near the surface and suggest an ejection from the boundary layer, followed by a strong viscous–inviscid interaction.

1. Introduction

The understanding of vortex motion in incompressible flows at high Reynolds number is a matter of increasing interest for environmental and industrial applications. The large effort required to calculate the Navier–Stokes solutions for such vortical flows, in particular, when boundaries are present, motivates many authors to search for an infinite-Reynolds-number asymptotic description of the vortical flow. The three-dimensional behaviour of vortex lines, as well as that of large-scale turbulent structures in a real fluid, has been studied by means of the computational methods for vortex filaments moving in an inviscid flow field. Many features of the interactions between vortex filaments are understood (Dhanak & De Bernardinis 1981; Chorin 1982; Siggia 1985; Winckelmans & Leonard 1988; Pedrizzetti 1992); more recently interactions with rigid bodies have been investigated (Walker 1978; Dhanak 1981; Doligalski & Walker 1984; Walker *et al.* 1987; Ersoy & Walker 1987; Pedrizzetti 1991*a*, *b*; Peridier, Smith & Walker 1991).

However, some physical processes associated with short-range interactions that are dominant in turbulent flows, such as the splitting and the reattachment of vortex tubes, as well as the bursting in boundary layers associated with the approach of vortex structures to solid boundaries (Smith *et al.* 1991), can be described only by taking into account the viscosity of the fluid.

The interaction of an infinitely long vortex filament with a rigid sphere, approaching from infinity, has been studied, in an incompressible inviscid flow, by Dhanak (1981), using the cutoff method. He defined a vortex image system in order to obtain a zero normal velocity on the surface of the body. The evolution of the filament, during the infinitely long period when the filament is approached with

constant speed by the body without being strongly deformed, has been computed by analytically solving a linear approximation of the equation of motion. Although it is not clear how to state the distance over which such an approximation is valid, a finite distance needs to be chosen as the initial condition for the numerical integration. A smooth evolution of the filament was obtained numerically, until the vortex gets so close to the sphere that the finite core of the vortex tube touches the surface of the body.

In the present work the evolution of an infinite vortex filament is investigated as it approaches a sphere that is fixed and embedded in a high-Reynolds-number flow. First, the problem has been investigated again by the cutoff method and the numerical solution shows the same features as already obtained by Dhanak (1981). Then the method is used to explore the complete inviscid evolution prior to core touching, regarding the cutoff only as a numerical regularization procedure. Then the results of the previous inviscid method are compared with those of a singular vortex (vorton) approach (Saffman 1980; Novikov 1983), which contains an intrinsic numerical viscosity (Pedrizzetti 1992) able to account for a viscous effect on the vortex structure evolution. In this case the vortex filament, after a short time of rapid stretching, does not loop around the sphere, as in the inviscid case, but breaks and becomes attached to the free-slip surface of the body owing to the reconnection with its image inside the sphere.

However, the inviscid description is incomplete, and in the limit of infinite Reynolds number when the vortex filament approaches the sphere surface, attachment is prohibited by the no-slip condition, and an unsteady boundary layer is expected to develop; in this layer a secondary vortex is generated and ultimately ejected to interact with the primary vortex filament (Harvey & Perry 1971; Blondeaux & De Bernardinis 1983; Walker *et al.* 1987).

A timescale analysis of the looping, the reattachment, and the secondary vortex generation is performed showing that a strong viscous–inviscid interaction, even when the filament is not very close to the body surface, must be expected to be the dominant feature of the flow field.

The three-dimensional boundary-layer separation and the beginning of the secondary vortex generation are calculated near the symmetry plane (Ersoy & Walker 1987) and flow patterns at the critical points are analysed (Perry & Fairlie 1974).

2. Ideal limit

2.1. *Presentation of the problem*

Consider a sphere of radius R, with its centre in the origin of a Cartesian system of coordinates, and a rectilinear filament, with circulation Γ, parallel to the Z-axis, intersecting the (X, Y)-plane at the point $(d^*+R, 0, 0)$. We make the problem dimensionless by choosing the unit of length L to be R and the unit of time T to be $4\pi R^2/\Gamma$. Thus the only dimensionless parameter in the problem is $d = d^*/R$, the non-dimensional initial separation of the filament from the body surface.

The filament is identified by its coordinate $\boldsymbol{X}_f(\xi, t)$, where t is the dimensionless time and ξ is a parametric coordinate, along the filament, chosen so that $\xi =$ constant always refers to the same fluid particle. The velocity induced by the filament at a point $\boldsymbol{x}$, distant from the filament itself, is obtained using the Biot–Savart law as

$$\boldsymbol{V}(\boldsymbol{x}) = -\int_{-\infty}^{+\infty} \frac{\boldsymbol{x}-\boldsymbol{X}_f(\xi',t)}{|\boldsymbol{x}-\boldsymbol{X}_f(\xi',t)|^3} \wedge \frac{\partial \boldsymbol{X}_f(\xi',t)}{\partial \xi'} \mathrm{d}\xi' + \boldsymbol{V}_e(\boldsymbol{x}), \tag{1}$$

where $\boldsymbol{V}_e(\boldsymbol{x})$ is the irrotational contribution to the velocity at $\boldsymbol{x}$ due to the image vorticity field within the sphere, required in order to satisfy the boundary condition of zero normal velocity on the sphere surface.

The integral in (1) diverges as $\boldsymbol{x} \to \boldsymbol{X}_f(\xi',t)$, because a vortex line of zero cross-section moves with infinite speed when its curvature is non-zero. For this reason a cutoff of the integral must be inserted, for practical purposes, when (1) is used to compute the velocity of the vortex itself. This corresponds, from the physical point of view, to assuming a finite core size in the filament, as will be described below.

2.2. *Image system*

The image system of a vortex element in a sphere has been given by Lighthill (1956), under the additional constraint that, if the vortex element is part of a solenoidal vortex field, the image vortex field is also solenoidal; this renders the solution unique. We briefly outline here the results applied to the present work.

Given an infinitesimal portion of the vortex filament centred at $\boldsymbol{x}$ of strength $\boldsymbol{\gamma} = \partial \boldsymbol{x}/\partial\xi \, \mathrm{d}\xi$ and denoting $r = |\boldsymbol{x}|$, the image system is given by:

(i) a vortex element at the inverse point $\boldsymbol{x}^* = \boldsymbol{x}/r^2$, of strength

$$\boldsymbol{\gamma}^* = \frac{2}{r}\left(\frac{(\boldsymbol{\gamma}\cdot\boldsymbol{x})}{r^2}\boldsymbol{x} - \tfrac{1}{2}\boldsymbol{\gamma}\right);$$

(ii) a line vortex of circulation $-(\boldsymbol{\gamma}\cdot\boldsymbol{x}/r)$ stretching from x^* to the centre of the sphere.

The velocity in a point $\boldsymbol{x}_p$, due to (i) is given by

$$\mathrm{d}\boldsymbol{V}_e^{(i)}(\boldsymbol{x}_p) = -\frac{(\boldsymbol{x}_p - \boldsymbol{x}^*) \wedge \boldsymbol{\gamma}^*}{|\boldsymbol{x}_p - \boldsymbol{x}^*|^3}; \tag{2}$$

the velocity due (ii) is

$$\begin{aligned} \mathrm{d}\boldsymbol{V}_e^{(ii)}(\boldsymbol{x}_p) &= -\frac{\boldsymbol{\gamma}\cdot\boldsymbol{x}}{r^2}\boldsymbol{x} \wedge \boldsymbol{x}_p \int_0^{1/r} \frac{\mathrm{d}\lambda}{|\boldsymbol{x}_p - \lambda\boldsymbol{x}/r|^3} \\ &= -\frac{\boldsymbol{\gamma}\cdot\boldsymbol{x}}{r^2}\boldsymbol{x} \wedge \boldsymbol{x}_p \frac{1}{4\alpha - \beta^2}\left[\frac{2\beta + 4/r}{((1/r^2) + (\beta/r) + \alpha)^{\frac{1}{2}}} - \frac{2\beta}{\alpha^{\frac{1}{2}}}\right]; \end{aligned} \tag{3}$$

where $\alpha = |\boldsymbol{x}_p|^2$ and $\beta = -(2/r)(\boldsymbol{x}_p\cdot\boldsymbol{x})$.

The filament is regarded as being closed by a semicircle of infinite radius. The velocity field due to (i) is of the order $\mathrm{d}\xi/r$. By expanding the velocity due to (i) in powers of $1/r$, we obtain

$$\mathrm{d}\boldsymbol{V}_e^{(i)}(\boldsymbol{x}_p) = -\frac{\boldsymbol{\gamma} \wedge \boldsymbol{x}_p}{r|\boldsymbol{x}_p|^3} + O\left(\frac{1}{r}\right)^2 \mathrm{d}\xi. \tag{4}$$

The first term on the right-hand side of (4) is $O(1/r)\,\mathrm{d}\xi$ and gives a null contribution when integrated along a closed path. Thus, when considering a closed filament, it can be subtracted from (2) to yield

$$\mathrm{d}\boldsymbol{V}_e^{(i)}(\boldsymbol{x}_p) = -\frac{(\boldsymbol{x}_p - \boldsymbol{x}^*) \wedge \boldsymbol{\gamma}^*}{|\boldsymbol{x}_p - \boldsymbol{x}^*|^3} + \frac{\boldsymbol{\gamma} \wedge \boldsymbol{x}_p}{r|\boldsymbol{x}_p|^3}. \tag{5}$$

As the two velocity fields due to (i) and (ii) defined in (3) and (5) are of $O(1/r)^2\,\mathrm{d}\xi$, they give a null contribution when integrated along the semicircular path of infinite radius, and the vortex elements can be distributed only on the open range $(-\infty, +\infty)$.

2.3. *Cutoff method*

In order to use (1) to compute the evolution of a filament in ideal flow we must introduce a suitable cutoff method for making the integral finite. Following Moore (1972) (see also Moore & Saffman 1972), Rosenhead's cutoff method is used here. This requires that the denominator of the integrand in (1) be replaced by a strictly positive function by introducing a cutoff parameter μ; in this way we obtain the modified Biot–Savart equation

$$\dot{\boldsymbol{X}}_{\mathrm{f}}(\xi,t) = -\int_{-\infty}^{+\infty} \frac{\boldsymbol{X}_{\mathrm{f}}(\xi,t)-\boldsymbol{X}_{\mathrm{f}}(\xi',t)}{(|\boldsymbol{X}_{\mathrm{f}}(\xi,t)-\boldsymbol{X}_{\mathrm{f}}(\xi',t)|^2+\mu^2)^{\frac{3}{2}}} \wedge \frac{\partial \boldsymbol{X}_{\mathrm{f}}(\xi',t)}{\partial \xi'}\,\mathrm{d}\xi' + \boldsymbol{V}_{\mathrm{e}}(\boldsymbol{X}_{\mathrm{f}}(\xi,t)). \tag{6}$$

Here μ represents a lengthscale characteristic of the filament cross-section, that, in the case of a circular section, is proportional to the core radius c. In particular, assuming that the vorticity is constant inside the core and zero outside, with no axial flow, and using the exact solution for the velocity of a circular vortex ring, the relation is

$$c = \mathrm{e}^{\frac{3}{4}}\mu. \tag{7}$$

The evolution of the filament core size, c, can be taken into account by considering the vortex volume conservation during stretching of the vortex lines. This consideration leads to a variation of c along the filament due to differential stretching. However Moore & Saffman (1972) showed that any variation in the internal structure along the filament produces an axial flow which smooths it out in a time that is short compared with the timescale associated with changes in the geometrical configuration of the filament. In the present case of an infinite vortex, this corresponds to maintaining the cutoff μ constant in time and along the filament. The cutoff constancy also ensures an Hamiltonian structure of the filament evolution equation (6) (Agishtein & Migdal 1986). For these reasons, even though when the filament is very close to the sphere the velocity of the filament due to the image is $O(c^{-1})$, that is the same order of magnitude as the axial flow (Pumir & Siggia 1987), in the present work we decided to assume the cutoff μ to be constant. In fact when the filament gets close to the sphere the core deforms and assumption (7) becomes a poor estimation; in addition the model (6) becomes questionable and the cutoff is regarded only as a numerical regularization procedure.

2.4. *Numerical approximations*

The last issue to be defined here is how to deal numerically with the infinite range of integration due to the infinite length of the vortex filament. The positions of portions of the vortex which are farther than a few radii of the sphere from the $Z = 0$ plane will not change significantly with respect to the central part of the filament and the curvature is approximately zero; the infinite portions of undisturbed filament $\pm[\xi_0, \infty)$, with $\xi_0 \gg 1$, make a contribution due to its image to the velocity in the central part of the filament of the order of $1/\xi_0$. With this in mind we choose a value $\xi_0 \gg 1$, with $1/\xi_0$ smaller than a defined precision (typically $\xi_0 \sim 10^5$) such that the two semi-infinite portions of filament $\pm[\xi_0, \infty)$ can be neglected. Then we choose another value ξ_1, with $\xi_0 \gg \xi_1 > 1$, such that in the two portions $\pm[\xi_1, \xi_0)$ the filament has a negligible curvature. Here the vortex self-induced velocity is also negligible and the

actual value of the core radius has little influence, such that it can assume values substantially different from the physical one without modifying the influence of these portions on the whole vortex motion. In these portions grid points are distributed with a spacing growing in a geometric progression $\Delta\xi_i = \alpha\Delta\xi_{i-1}$, also implying, as will be clear below, a geometric growth of the cutoff length. Finally, in the internal region $(-\xi_1, +\xi_1)$, we distribute the computational points in order to have the desired resolution and reproduce correctly the actual core size. This procedure permits an accurate description using a reasonable number of points, provided the radius of curvature is everywhere much larger than the grid point spacing, and the point ξ_1 is well outside the range of interest.

A grid point intersection procedure has been implemented in order that the ratio between grid spacing, Δx, and cutoff length, in the central region, $\Delta x/\mu < 1.5$. This ensures an error in the evaluation of the self-induced velocity of less than 3%, as compared with the exact solution for a thin circular ring, for a ratio between radius of curvature and core size of greater than 5. The new point is inserted automatically by computing a second-order best approximation of the nearest four points. The value of ξ_1 has been fixed to 3 and the parameter $\alpha = 1.5$; in this way we arrive at $\xi_0 \approx 10^5$ with about 200 grid points. The values of the numerical parameters have been chosen after a extensive sensitivity study, part of which is reported in Pedrizzetti (1991*a*).

The strongest contribution to the velocity field in (6) is given by the contribution of the image vortex. The vortex velocity due to the image system is of $O(1)$ initially and becomes $O(c^{-1})$ when the vortex core touches the sphere; the vortex self-induced velocity is much smaller and ranges respectively from 0 to 1. The strong influence of images has required a careful time integration, while the introduction of the expansion of the integrand in (6) near the computational points (Dhanak & De Bernardinis 1981; Ersoy & Walker 1987) to improve accuracy and avoid instabilities of the weaker contribution proved unnecessary.

The numerical integration is carried out using a fourth-order Runge–Kutta time advancement with a variable time step. The maximum time step is taken as $\mathrm{d}t = 2 \times 10^{-3}$, and equal to the dimensionless maximum displacement of a grid point in one step, so that the actual time step used is always much smaller than $\mathrm{d}t$ after the initial period.

2.5. *Calculated results*

The value of the initial distance between the filament and the sphere surface, d, does not influence the qualitative picture of the close vortex–body interaction; indeed we observed that when the vortex starts a large distance from the sphere, it always evolves to a configuration in which the distance is comparable with the sphere radius (say $d \sim 1$), with the filament only slightly deformed (that is its radius of curvature is much larger than one). For this reason we focus our attention on a unique initial configuration with $d = 1$, in order to observe a typical close interaction the filament with the body.

During this research work we performed several simulations with core size c varying from 0.05 to 0.2. The value $c = 0.1$ ($\mu \approx 0.0472$) was then fixed since the qualitative picture of the interaction does not change. This small value is considered sufficient for the accuracy of the model described by the evolution equation (6), which is accurate only in the limit of radius of curvature of the filament, here expected to be $O(1)$, much larger than the cutoff value (Moore & Saffman 1972).

As expected from the previous works of Dhanak (1981) and Pedrizzetti (1991*a*) the central part of the filament starts to move around the sphere, creating a non-zero

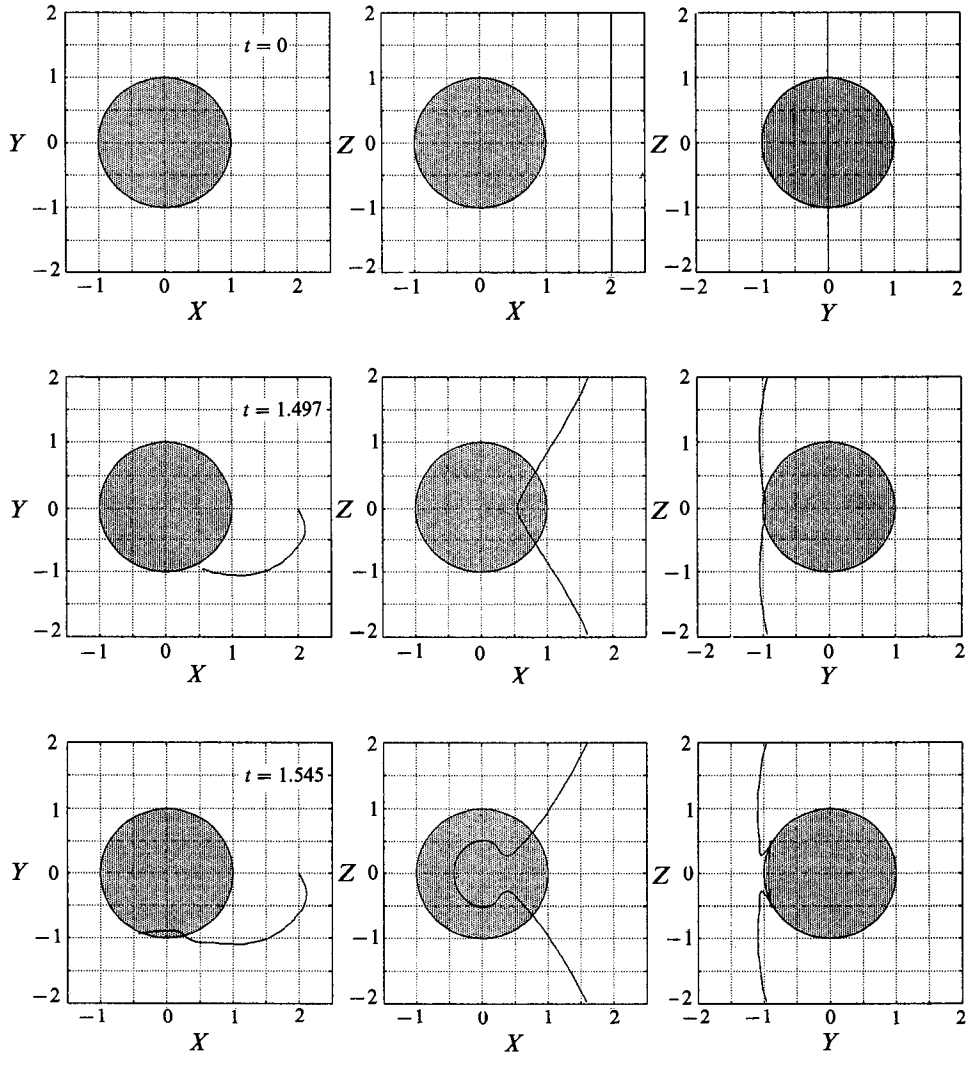

FIGURE 1. Evolution of an ideal vortex filament, of core radius 0.1, starting a distance $d = 1$ from a sphere. Top view, side view, and end view are shown from left to right, at times $t = 0$; $t = 1.497$; and $t = 1.545$.

curvature, and then the self-induced velocity leads it toward the body surface. When it arrives very close to the surface it rapidly stretches over the sphere and acquires a significant perturbation due to the body surface shape. The initial evolution of the vortex filament is shown in figure 1. At time $t = 1.545$ the vortex core has already touched the surface of the sphere; however the integration is continued to explore the complete inviscid evolution after the core has touched, regarding the cutoff only as a numerical regularization procedure. Thereafter the central portion of the filament stretches rapidly over the sphere until two symmetric points in the vortex, initially distant, touch each other. After this point the computation cannot continue because of the ideal model. A three-dimensional sketch of the final vortex configuration is given in figure 2.

This result provides only an approximation of the actual ideal evolution, as discussed above, because of the unknown real evolution of the transverse filament

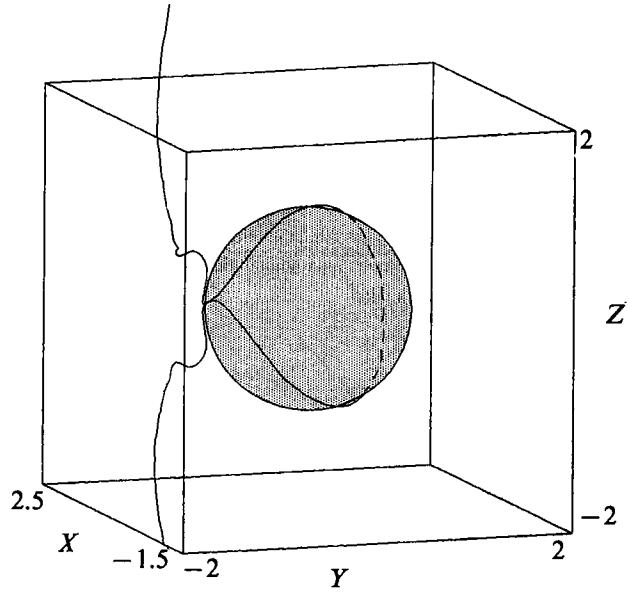

FIGURE 2. Looping of an ideal vortex filament of core radius 0.1, around a sphere initially at a distance $d = 1$; axonometric projection at time $t = 1.582$.

section. However, the qualitative independence from the core radius value strongly suggests the possibility that when a thin vortex filament comes in close contact with a sphere (in an ideal fluid) it gives rise to an highly stretched vortex ring, which, in the presence of a slight dissipative effect, will eventually detach, leaving the body taking a net impulse from the vortex structure.

3. Viscous evolution on free-slip surface

3.1. *Method of solution*

In the previous section we observed the ideal evolution of the vortex filament, and inferred that a slight viscous effect can permit some topological change to be seen in the vortex structure. The first step in order to extend the results to include viscosity can be accomplished by considering the presence of a viscous effect in the vortex structure evolution, still without taking into account the influence of the viscous boundary layer on the outer flow. In order to do this we consider the vortex singularities (vorton) method.

The vorton method is very similar to the cutoff method described above, the main difference being in the fact that the integral (1) is discretized *a priori* and the computational points along the filament are not *ordered*; that is the parametric coordinate ξ is used only to define the initial configuration of the filament and then forgotten. The vorton method has been introduced by Saffman (1980) and Novikov (1983) (see also Aksman, Novikov & Orszag 1985; Pedrizzetti 1992, for further developments), and we briefly outline here the model as used in the present work.

Consider an initial configuration of the vortex filament $\boldsymbol{X}_f(\xi)$ and assume a discretization of the parameter space ξ, with $\Delta\xi^{(\alpha)} = \xi^{(\alpha+1)} - \xi^{(\alpha)}$ small but finite. Define the position of the centre and the intensity of the αth portion of filament respectively as

$$\boldsymbol{x}^{(\alpha)} = \boldsymbol{X}_f(\tfrac{1}{2}(\xi^{(\alpha)} + \xi^{(\alpha+1)})); \quad \boldsymbol{\gamma}^{(\alpha)} = (\partial \boldsymbol{X}_f(\xi)/\partial\xi)^{(\alpha)}\, \Delta\xi^{(\alpha)}. \tag{8}$$

The vortex filament structure can be discretized by a number N of vortex singularities, located at $\boldsymbol{x}^{(\alpha)}$, of intensities $\boldsymbol{\gamma}^{(\alpha)}$, $\alpha = 1, 2, \ldots, N$:

$$\boldsymbol{\omega}(\boldsymbol{x}, t) = \sum_{\alpha=1}^{N} \boldsymbol{\gamma}^{(\alpha)} \delta(\boldsymbol{x} - \boldsymbol{x}^{(\alpha)}), \tag{9}$$

with $\delta(\cdot)$ being the Dirac delta function. Once the singularities are defined by (8) they are assumed to be independent and the parametric coordinate ξ is abandoned. The vortex field (9) induces a velocity field at any point $\boldsymbol{x}^{(\alpha)}$ that can be computed by means of the Biot–Savart law to yield

$$\boldsymbol{u}(\boldsymbol{x}^{(\alpha)}) = \dot{\boldsymbol{x}}^{(\alpha)} = -\sum_{\substack{\beta=1 \\ \beta \neq \alpha}}^{N} \frac{(\boldsymbol{x}^{(\alpha)} - \boldsymbol{x}^{(\beta)}) \wedge \boldsymbol{\gamma}^{(\beta)}}{|\boldsymbol{x}^{(\alpha)} - \boldsymbol{x}^{(\beta)}|^3} + \boldsymbol{V}_{\mathrm{e}}(\boldsymbol{x}^{(\alpha)}), \tag{10}$$

where the dot denotes differentiation with respect to time.

Equation (10) represents a discrete version of (1) in which the cutoff is given by the omission of the $\alpha = \beta$ term. A difference lies in the fact that the loss of the parametric coordinate ξ does not permit the computation of the derivative term present in the integrand of (1), which is substituted by $\boldsymbol{\gamma}$ in (10). For this reason an equation for the evolution of the intensity vector must now be introduced. Substituting (9) and (10) into the vorticity equation for an inviscid flow

$$\mathrm{d}\boldsymbol{\omega}/\mathrm{d}t = (\boldsymbol{\omega} \cdot \boldsymbol{\nabla})\, \boldsymbol{u}, \tag{11}$$

gives the equation for the evolution of the vorton intensities

$$\dot{\boldsymbol{\gamma}}^{(\alpha)} = \boldsymbol{\gamma}^{(\alpha)} \cdot \boldsymbol{\nabla} \boldsymbol{u}(\boldsymbol{x}^{(\alpha)}). \tag{12}$$

The cutoff, implicit in this formulation of the problem defined in (1), has a lengthscale equal to the distance, Δx, between vortex singularities. In this way a uniform core size proportional to the cutoff length is implicitly assumed giving an equation analogous to (7) (Pedrizzetti 1992):

$$c \approx 0.875 \Delta x. \tag{13}$$

A major problem of this formulation is the core evolution. In fact, following (13), the core size increases during stretching of vortex lines; for this reason a dividing vortex procedure is introduced in order to maintain the core size constant on average (see Pedrizzetti 1992, for estimates of the approximation).

The vortex system as defined in (9) is not divergence free (even though a divergence-free vorticity field can be reconstructed by taking the curl of (10)). Nevertheless, when we approximate (1) or (6) with a quadrature formula we also deal with a non-divergence-free vortex representation which well approximates the continuous filament structure. The main difference in the cutoff method is that the parametric representation introduces an order to the grid points which makes the method self-consistent in representing a continuous structure. In the vorton method the independence of singularities requires a different approach such as the self-consistent filter introduced by Pedrizzetti (1992).

The independence of the vortex singularities from a defined topological vortex configuration makes this model less accurate for simulating an ideal flow evolution. In fact the model introduces implicitly a viscous effect in vortex motion during moments of rapid stretching. This implies an inherent regularization of the motion

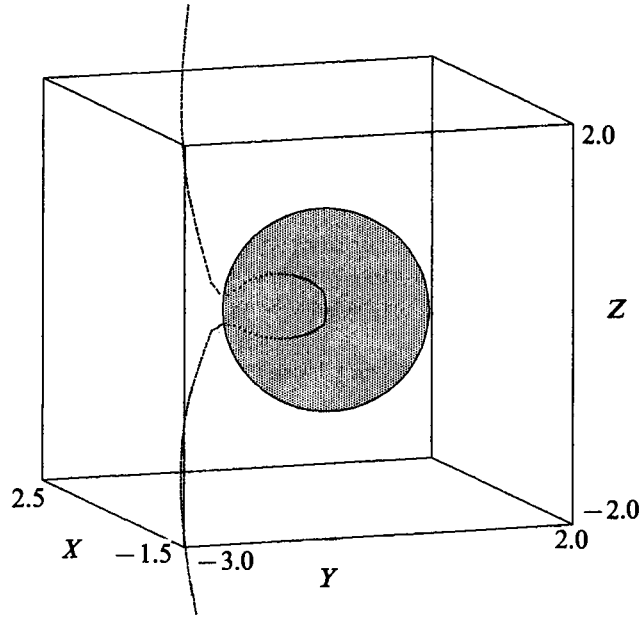

FIGURE 3. Reattachment of a viscous filament of core radius 0.1, over a free-slip sphere surface, initially at a distance $d = 1$; axonometric projection at time $t = 1.556$. The image vortex is sketched inside the sphere.

and permits the reproduction of vortex reconnection, otherwise impossible, without observing high velocity gradients (Aksman & Novikov 1988; Pedrizzetti 1992). The value of this numerical viscosity has been estimated by Pedrizzetti (1992) as

$$\nu \sim c\,\mathrm{d}L/\mathrm{d}t \tag{14}$$

where $\mathrm{d}L/\mathrm{d}t$ is the stretching rate of a vortex line. During moments of vortex reconnection, the stretching increases strongly, and this viscosity rapidly approaches $O(1)$ values, permitting the observation of a rapid reconnection. The derivation of (14) and a quantitative comparison with existing results on vortex reconnection are reported in Pedrizzetti (1992).

The numerical discretization and integration is the same as described in §2 for the cutoff method, with $\mathrm{d}t = 10^{-3}$.

3.2. *Calculated results*

Several simulations have been performed with this method, showing a good agreement with the results of §2 up to the time the filament comes very close to the sphere.

When the filament arrives in the immediate vicinity of the sphere it is subjected to a rapid stretching. This makes the intrinsic viscous effect very important and we observe, very soon the vortex splitting into two parts, terminating on the free-slip surface of the sphere. This phenomenon is due to the presence of the image vortex inside the sphere, and, in absence of no-slip condition on the surface, the external vortex reconnects with its internal image, in analogy with the classical phenomenon of reconnection between real vortex structures. Figure 3 is a sketch of the vortex configuration after reattachment for $d = 1$ and $c = 0.1$; the image vortex is also sketched. This model reproduces the reconnection process spuriously because the

viscous effect (14) is unphysical. Thus it gives no idea of the time needed for the real process to develop, which depends of course on the real Reynolds number of the flow.

3.3. *Timescales analysis*

At this level of analysis we have observed two possible behaviours of the outer flow – the looping described in §2 and the reattachment of the present section – but we cannot be sure which one is the dominant process. For this reason we perform a timescale analysis for the phenomena described above in order to predict which of the possible processes actually dominates the external motion, at high Reynolds number, when the influence of the viscous boundary layer on the body surface is neglected.

Both the looping and the reattachment phenomena are composed of two different phases. During the first phase, which is common for both processes, the filament approaches the body surface, before starting the second phase of close interaction with the body itself characterized by intense stretching and terminating with different phenomena.

The characteristic time of approach, T_a, in our simulation is observed to be

$$T_a \approx 1.5; \tag{15}$$

such a timescale is usually easy to estimate in different situations. The time for complete looping to develop, T_l, is estimated from the results of §2 as

$$T_l \approx 0.1. \tag{16}$$

The reattachment time can be estimated by using a model for reconnection of two vortex filaments of opposite circulation. The order of magnitude can be obtained from Meiron *et al.* (1988), which in our units gives

$$T_{r0} \sim \tfrac{1}{8} \log Re, \tag{17}$$

where Re is the Reynolds number. A more accurate estimation can be obtained from the Saffman (1989) model where the complete reconnection is characterized by a rejoining time, T_{r2}, depending on geometric characteristics, and a complete connection time T_{r1}. In our units we can write

$$T_{r2} \approx \tfrac{1}{2} c^{\frac{1}{3}} \approx 0.16; \tag{18}$$

$$T_{r1} \approx \tfrac{5}{4} c^{\frac{5}{3}} [\log (Re(2/\pi)\, c^{\frac{1}{3}})]^{\frac{1}{3}}; \tag{19}$$

the time T_{r1} ranges from 0.25, for $Re = 10^6$, to 0.12 for $Re = 10^2$; these values are somewhat smaller than what is given by (17).

These figures suggest that the process of reattachment, when the Reynolds number is high enough, is slightly slower than the looping. When the Reynolds number is smaller than about 100 the two timescales of the processes are comparable, and both phenomena can be expected at the same time. The above estimations also suggest that, in the case of a free-slip plane boundary, only the reattachment can be expected.

The phenomena described in the previous sections do not take into account the no-slip boundary condition on the body surface, which prohibits, in a real flow, the termination of a vortex line on a solid wall. However, in the limit of very high Reynolds number, when the vortex filament approaches the sphere, it is expected

that the flow induced at the wall develops an unsteady boundary layer. Such a layer can eventually separate, growing till a secondary vortex of opposite circulation is generated within the boundary layer itself and ejected to interact, by pairing, with the primary vortex filament. This behaviour has been observed experimentally (Harvey & Perry 1971; Blondeaux & De Berndardinis 1983; Walker *et al.* 1987) and found theoretically (Walker 1978; Peace & Riley 1983; Ersoy & Walker 1987). From these works, we can estimate the timescale for the occurrence of this rebouncing process. We found the final time, when the pairing process has occurred, T_b, to range approximately between 0.2 and 0.5, which is comparable to the approach time. This characteristic time suggests that, at high Reynolds numbers, when the no-slip boundary condition must be satisfied and reattachment cannot exist, looping is unable to develop because of the quickness of the rebouncing process.

This timescale analysis shows that, in the limit of large Reynolds number, the boundary-layer evolution is driven by an outer field which is essentially inviscid, until an ejection from the boundary layer causes a strong viscous–inviscid interaction, dominating the subsequent evolution of the flow field.

4. Boundary-layer formulation

As the external inviscid vortex moves it induces an unsteady vortex-driven three-dimensional boundary layer, whose accurate description with a full numerical simulation would require very large computer resources for the Reynolds number we are interested in.

We followed the approach proposed by Ersoy & Walker (1987) that allows the computations of the leading term for all three components of the boundary-layer velocity field on and near the symmetry plane, $Z = 0$.

Consider the three-dimensional Navier–Stokes equations written in spherical coordinates (Batchelor 1967; Pedlosky 1979) with r, ϕ, θ as the radial, azimuthal and zenithal coordinates respectively, where $\theta = 0$ represents the equatorial plane, and the meridian given by $\phi = \pi$ faces the filament initial position; the respective velocities are w, u, and v. Let us define the following scaled variables:

$$\tilde{y} = (r-1)Re^{\frac{1}{2}}, \quad \tilde{w} = wRe^{\frac{1}{2}}; \tag{20}$$

where the Reynolds number $Re = \Gamma/(4\pi\nu)$.

Near the symmetry plane, $\theta \to 0$, we have $v = O(\theta)$, $u = u(\phi, \tilde{y}, t) + O(\theta^2)$, and $w = w(\phi, \tilde{y}, t) + O(\theta^2)$. The three-dimensional boundary-layer equations, with these variables, near the symmetry plane are

$$\frac{\partial v}{\partial t} + u\frac{\partial v}{\partial \phi} + \tilde{w}\frac{\partial v}{\partial \tilde{y}} + v\frac{\partial v}{\partial \theta} + u^2 \tan\theta = -\frac{\partial p_\infty}{\partial \theta} + \frac{\partial^2 v}{\partial \tilde{y}^2}, \tag{21}$$

$$\frac{\partial u}{\partial t} + u\frac{\partial u}{\partial \phi} + \tilde{w}\frac{\partial u}{\partial \tilde{y}} = -\frac{\partial p_\infty}{\partial \phi} + \frac{\partial^2 u}{\partial \tilde{y}^2}, \tag{22}$$

$$\frac{\partial v}{\partial \theta} + \frac{\partial u}{\partial \phi} + \frac{\partial \tilde{w}}{\partial \tilde{y}} = 0. \tag{23}$$

Here p_∞ is the pressure distribution due to the vortex filament evaluated at the edge of the boundary layer. In (21) all the terms are of order θ, while in (22) and (23) the terms are of order one with respect to the variable θ.

Near the symmetry plane the zenithal velocity, v, can be written as

$$v = g(\phi, \tilde{y}, t)\,\theta + O(\theta^3), \tag{24}$$

where $g = (\partial v/\partial\theta)_{\theta=0}$. Solving for the pressure terms, using (21), (22) at the edge of the boundary layer, $\tilde{y} \to \infty$, and substituting (24) into (21)–(23) we obtain a set of equations describing the unsteady boundary layer on the symmetry plane,

$$\frac{\partial g}{\partial t} + u\frac{\partial g}{\partial \phi} + \tilde{w}\frac{\partial g}{\partial \tilde{y}} + g^2 + u^2 = \frac{\partial g_\infty}{\partial t} + u_\infty \frac{\partial g_\infty}{\partial \phi} + g_\infty^2 + u_\infty^2 + \frac{\partial^2 g}{\partial \tilde{y}^2}, \tag{25}$$

$$\frac{\partial u}{\partial t} + u\frac{\partial u}{\partial \phi} + \tilde{w}\frac{\partial u}{\partial \tilde{y}} = \frac{\partial u_\infty}{\partial t} + u_\infty \frac{\partial u_\infty}{\partial \phi} + \frac{\partial^2 u}{\partial \tilde{y}^2}, \tag{26}$$

$$\frac{\partial u}{\partial \phi} + g + \frac{\partial \tilde{w}}{\partial \tilde{y}} = 0; \tag{27}$$

with the boundary conditions

$$\tilde{w} = u = 0, \quad g = 0 \quad \text{at} \quad \tilde{y} = 0, \tag{28}$$

$$u \to u_\infty, \quad g \to g_\infty \quad \text{as} \quad \tilde{y} \to \infty, \tag{29}$$

and periodicity in the ϕ-direction.

For the numerical integration of (25)–(27) we introduce a stretched radial coordinate, $\eta = \log(\tilde{y} + a/a)$, ensuring a better resolution in the vicinity of the wall, where the parameter a determines the rate of coordinate stretch.

Substituting the coordinate η for the coordinate $\tilde{y}$ in (25)–(29), we can write the set of equations as

$$\frac{\partial g}{\partial t} + u\frac{\partial g}{\partial \phi} + \tilde{w}\frac{\partial g}{\partial \eta}\frac{1}{ae^\eta} + g^2 + u^2 = \frac{\partial g_\infty}{\partial t} + u_\infty \frac{\partial g_\infty}{\partial \phi} + g_\infty^2 + u_\infty^2 + \frac{1}{(ae^\eta)^2}\left(\frac{\partial}{\partial \eta^2} - \frac{\partial}{\partial \eta}\right) g, \tag{30}$$

$$\frac{\partial u}{\partial t} + u\frac{\partial u}{\partial \phi} + \tilde{w}\frac{\partial u}{\partial \eta}\frac{1}{ae^\eta} = \frac{\partial u_\infty}{\partial t} + u_\infty \frac{\partial u_\infty}{\partial \phi} + \frac{1}{(ae^\eta)^2}\left(\frac{\partial^2}{\partial \eta^2} - \frac{\partial}{\partial \eta}\right) u, \tag{31}$$

$$\frac{\partial \tilde{w}}{\partial \eta} = -ae^\eta\left(\frac{\partial u}{\partial \phi} + g\right), \tag{32}$$

which we then solved numerically with the boundary condition (28) imposed at $\eta = 0$ and the condition (29) imposed, numerically, at a large, but finite, value $\eta = \eta_{\max}$.

The numerical integration of (30)–(32) is performed by solving, at each time step, the filament motion with the cutoff method as described in §2, computing the velocity u, and the gradient g, on the wall using (1), then taking these values, u_∞ and g_∞ respectively, as the boundary condition at infinity for the boundary-layer formulation. Then the boundary-layer equations are solved with a simple finite-difference method, assuming an impulsively started initial condition, which corresponds to an abrupt creation of the vortex filament in its initial configuration.

The stretched radial coordinate permits the large numerical gradients which appear in proximity of the wall after the impulsive start to be followed. This has been monitored by comparing the circulation around the sphere on the $\theta = 0$ plane, as induced by the external inviscid vortex, and as given by the separated vorticity; these quantities become indistinguishable after few initial time steps.

The system has been integrated with an implicit Adams–Bashforth second-

order scheme. In the following computation we used used the parameter $a = 0.5$, $\eta_{\max} = 4$.

5. Boundary-layer evolution

5.1. $d = 1$

In the study of the boundary-layer evolution we can expect, as opposed to the free-slip evolution, a qualitative dependence of the results on the initial separation, d, between the vortex filament and the sphere surface. The first case studied, for continuity with the preceding results, is for the initial separation $d = 1$. In this configuration we performed two different simulation, with varying grid, using a 128×64 grid and a 64×36 grid in the ϕ- and η-directions respectively. The two simulations are absolutely indistinguishable until the last stage of the simulation ($t \geqslant 0.2$), when large gradients appear and the greater resolution of the first mesh allows the simulation to continue a little longer.

The three-dimensional motion in the boundary layer is complex and in order to have a sensible picture of the flow field we give three different plots: (*a*) a contour plot of the vertical vorticity, $\omega = \partial u/\partial \eta$, on the symmetry plane; (*b*) a contour plot of the gradient, g, on the symmetry plane; and (*c*) limiting streamlines on the sphere surface, the (ϕ, θ)-plane, close to the symmetry plane.

The vortex filament induces on the boundary layer a vortex field, of opposite sign, varying in the tangential direction. For $t = 0$ there is a symmetry between the $(0, \pi)$ and $(\pi, 2\pi)$ ranges of ϕ. After a short time an unsteady boundary layer begins to develop, disrupting the symmetry. The vorticity field elongates from the boundary, turning and reducing the amount of vorticity on the left and of the central nucleus, as depicted in figure 4(*a*). The gradient of zenithal velocity, g, represents the outflow ($g > 0$), or inflow ($g < 0$), from and into the symmetry plane. In figure 4(*b*), the contour plot of g is reported at $t = 0.1$. The $g = 0$ contours (dash-dot line), leaving the boundary, divide the inflow (dashed lines) and outflow (continuous lines) regions; we can see the onset of outflow close to the boundary, corresponding to tangential velocity slowdown, apart from a small central region of persistent, relatively weak inflow. From this picture, the variations of the g- field in the radial direction suggest the appearance of streamwise vorticity of opposite sign above and below the symmetry plane, but the whole vorticity field in the ϕ- and $\tilde{y}$-directions cannot be evaluated within the present approximation. The limiting streamlines, plotted in figure 4(*c*), show a wavy motion with a maximum in the tangential velocity at about $\phi = \pi$. The vorticity field at $t = 0.2$, figure 5(*a*), presents an elongation from the boundary and a compression of the erupting vorticity, while a small vorticity region of opposite sign appears on the boundary at about $\phi = 0.85\pi$. The development of the gradient, g, is depicted in figure 5(*b*). The small inflow region still persists and a localized important outflow structure appears at $\phi \approx 0.76\pi$, corresponding to a separating vortex which encloses a focus. A similar local structure of the vertical flow was also observed in an infinite flat boundary layer driven by an inclined vortex ring (Ersoy & Walker 1987) but it is interesting to notice that in this case the sign is opposite, because of the closed boundary structure. The corresponding limiting streamlines, figure 5(*c*), show a first inversion of the tangential velocity, at $\phi = 0.79\pi$, where a strong outflow is present, with the onset of a radial outflow. On the right of this point, the tangential velocity changes sign again, corresponding to a relatively weak inflow. The subsequent local development can be observed in figure 6, at $t = 0.225$, which shows an enlarged view of this region in the (ϕ, η)-plane. The

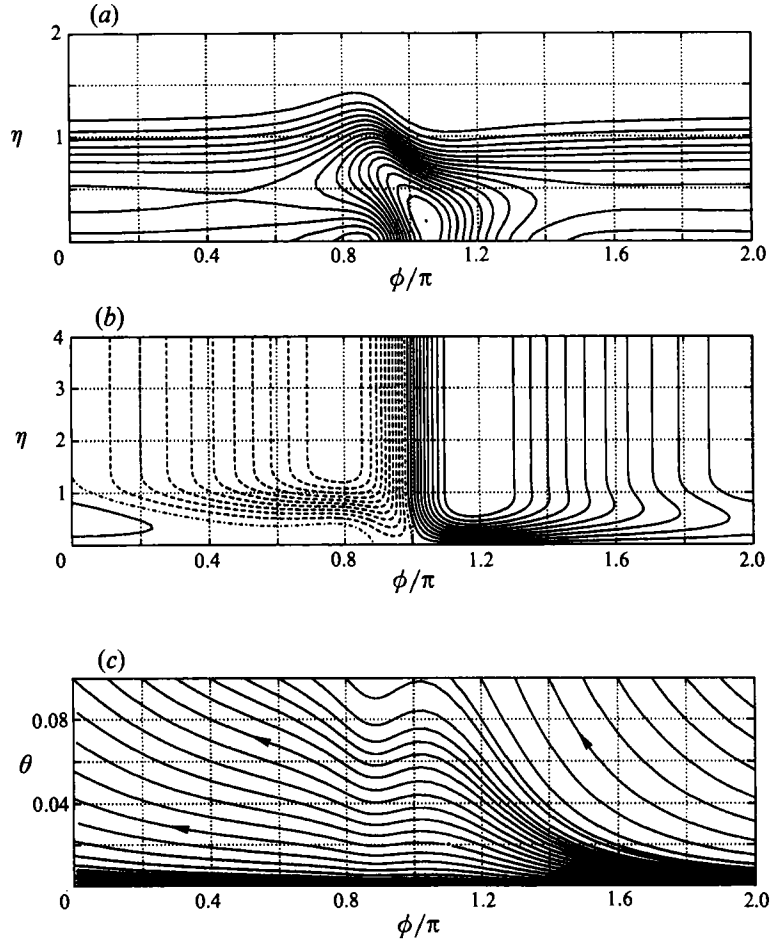

FIGURE 4. Vortex-induced boundary-layer development at $t = 0.1$, for initial vortex distance $d = 1$. (*a*) Vorticity contours, levels from -9 to -0.5, step 0.5; (*b*) spanwise velocity gradient contours, levels from -2.5 to -0.25, step 0.25 (– – –); level 0 (— · — · —); levels from 0.25 to 2.5, step 0.25 (——); (*c*) limiting streamlines on the wall.

streamlines on the symmetry plane are shown, with the superimposed $g = 0$ contour (dash-dot line) separating the inflow and outflow regions. A complete secondary vortex structure, which actually appeared before $t = 0.175$, is clearly recognized, and is associated with a focus of strong flow out of the symmetry plane. The streamline patterns may be considered to be representative of a transverse section of a three-dimensional separating vortex (Smith *et al.* 1991). The vortex is confined, at the wall, by two stagnation points. A stagnation point of attachment on the sphere surface is localized at $\phi = 2.39$, characterized by a strong outflow in the θ-direction, while there is a stagnation point of separation at $\phi = 2.87$ with a weak inflow from the third dimension. This type of separation is similar to that observed in two-dimensional separation induced by a vortex flow (Walker 1978; Peace & Riley 1983; Doligalski & Walker 1984; Peridier *et al.* 1991), the main difference lies in the fact that the streamlines do not form closed loops but spiral toward the focus to leave the symmetry plane. In figure 7 we show a three-dimensional view of streamlines, selected from figure 6 but starting slightly above the symmetry plane. From this we can capture the three-dimensional structure of the separating vortex near the

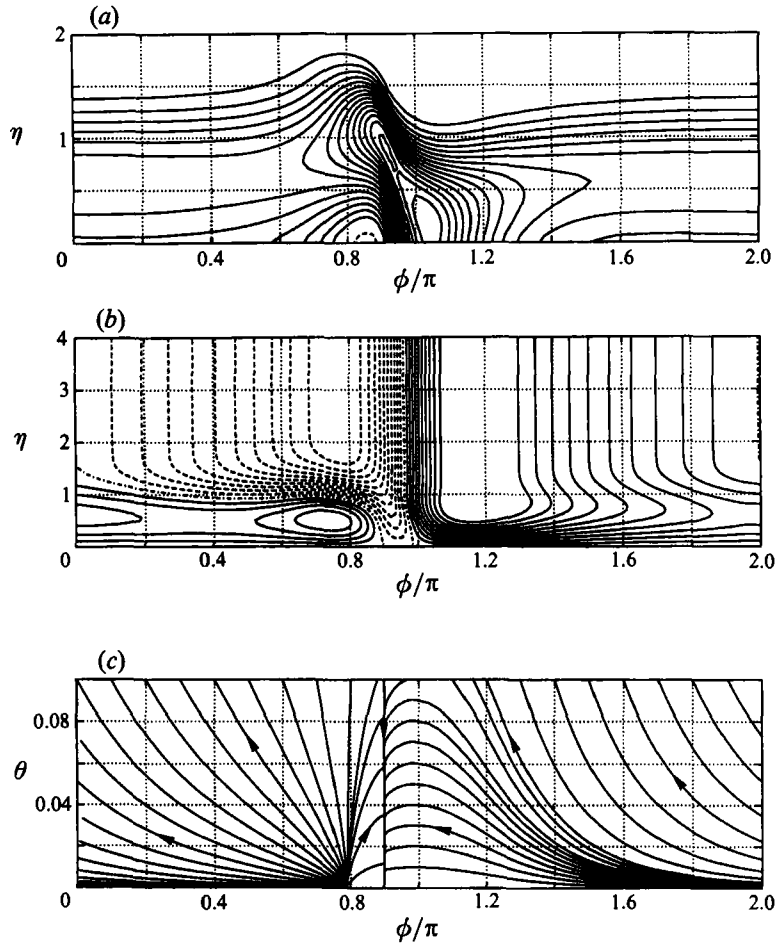

FIGURE 5. Vortex induced boundary layer development at $t = 0.2$, for initial vortex distance $d = 1$. (*a*) Vorticity contours, levels from -8 to -0.5, step 0.5 (——); level 0.5 (– – –); (*b*) spanwise velocity gradient contours, levels from -2.5 to -0.25, step 0.25 (– – –); level 0 (— · — · —), levels from 0.25 to 2.5, step 0.25 (——); (*c*) limiting streamlines on wall.

symmetry plane, with streamlines spiralling toward the focus moving in the third dimension. After this time the flow presents increasingly strong spatial gradients, and the numerical scheme becomes inadequate, failing to converge after $t = 0.26$. It is worth noticing that the vortex distance from the sphere surface is reduced from $d = 1$ only to 0.96. The numerical results suggest the development of a singular behaviour of the viscous wall flow in finite time. A singularity is known to occur on the symmetry plane of a three-dimensional unsteady boundary layer when the separation line on the surface of the body crosses the symmetry plane normally (Van Dommelen & Cowley 1990; Van Dommelen 1990). During and after the three-dimensional separation a complete viscous–inviscid interaction of the boundary layer with the external vortex structure should be taken into account.

5.2. $d = 3$

In this configuration we performed the simulation using a 64×36 grid in the ϕ- and η-directions respectively, this lower resolution having been shown in the previous case to give an accurate description of the flow field, the only limitation being that

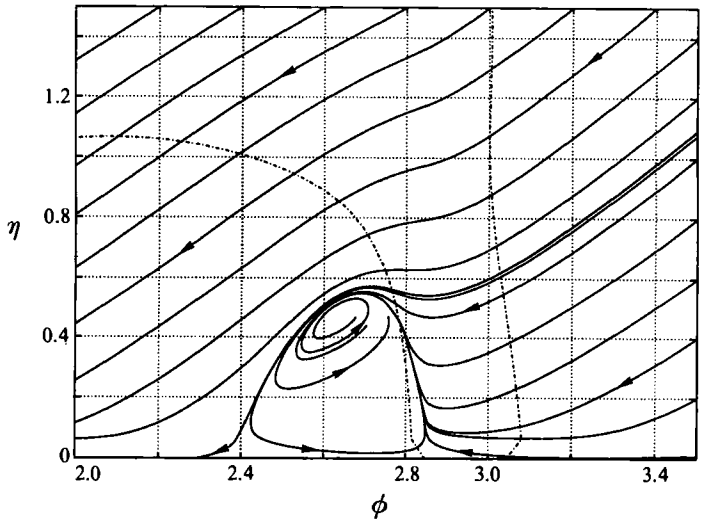

FIGURE 6. Enlarged view of the vortex-induced boundary-layer development at $t = 0.225$, for initial vortex distance $d = 1$. Streamlines on the symmetry plane are shown (——) with superposed spanwise velocity gradient zero contour (– – – –).

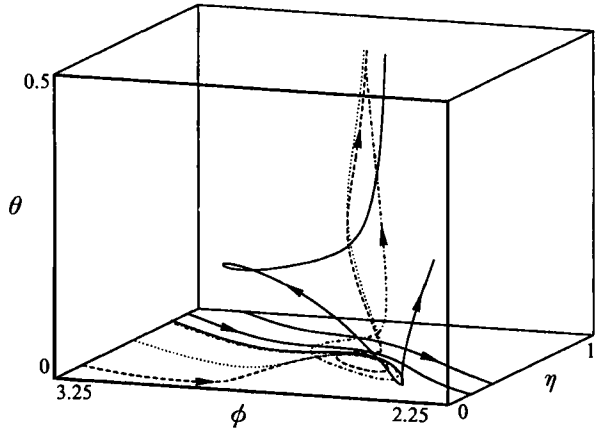

FIGURE 7. Enlarged view of the vortex-induced boundary-layer development at $t = 0.225$, for initial vortex distance $d = 1$. Axonometric view of selected streamlines.

the mesh becomes inadequate a little sooner than with a more resolved grid at the final stage of the simulation; on the other hand it permits a long simulation to be performed, as it is in this case, with still affordable computational effort.

The boundary-layer timescale is, in our units, $T_{\mathrm{bl}} \sim 1$, and this represents the time needed by the boundary layer to readjust to an external forcing; the timescale of the forcing, given by the filament, is given by its radius of curvature (or by the square of the distance, if it is smaller) which is much greater than 1, so while the forcing is weak enough that a steady boundary-layer solution exists, the boundary layer has time to readjust to a stable quasi-steady equilibrium configuration. In the present physical problem, an important unsteady boundary layer starts to grow only after the filament is within a critical distance of the sphere surface, which can be estimated to be about 2. An analogous phenomena was found by Walker *et al.* (1987), for the impact of a vortex ring on a wall; they showed that an important unsteady

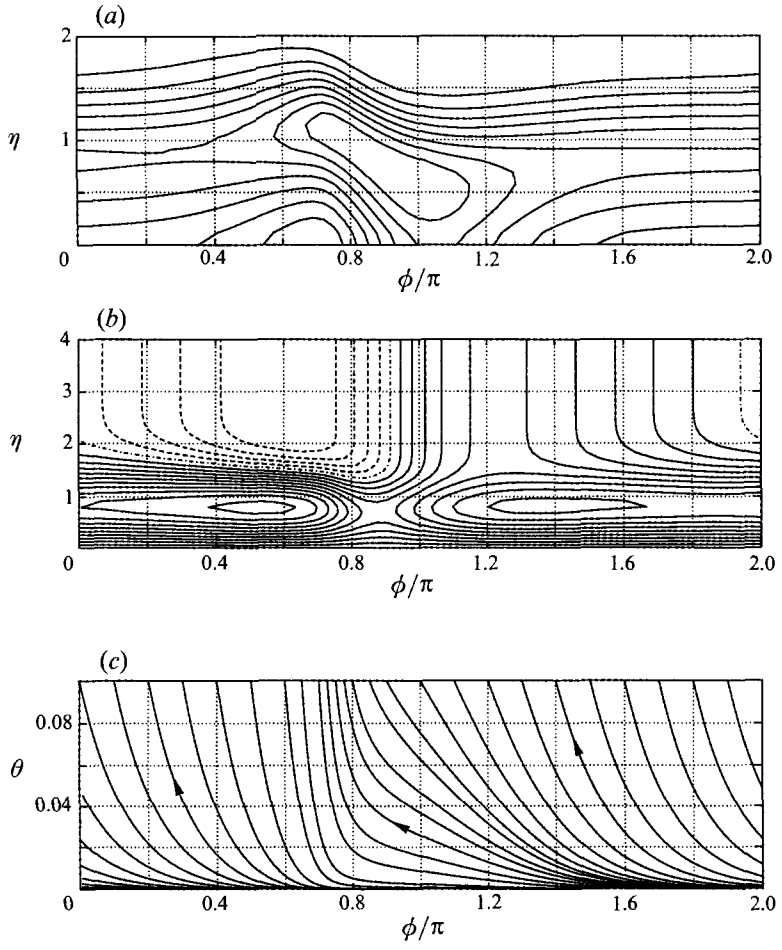

FIGURE 8. Vortex-induced boundary-layer development at $t = 6$, for initial vortex distance $d = 3$. (*a*) Vorticity contours, levels from -4 to -0.5, step 0.5; (*b*) spanwise velocity gradient contours, levels from -1 to -0.25, step 0.25 (----); level 0 (—·—·—); levels from 0.25 to 2.5, step 0.25 (——); (*c*) limiting streamlines on the wall.

boundary-layer effect starts to develop after the ring has approached the wall within a distance comparable with its diameter.

As the filament starts to evolve, a vorticity field of opposite sign starts to develop, as in the previous case, until, for $t \approx 1$, the evolution slows down to a quasi-steady configuration. In figure 8 the boundary-layer structure is reported at time $t = 6$; at this time the vortex distance from the sphere surface is reduced from $d = 3$ to 2.38. The global structure has not changed qualitatively from the configuration at $t = 1$, and little even quantitatively along with the external forcing. The vorticity contours in figure 8(*a*) (graphic inaccuracy is due to representing a contour, on a coarse grid, of a slowly varying function) show a quite diffused field, as compared with the preceding case. A peculiar characteristic of such an equilibrium solution is the onset of outflow close to the surface in a complete annulus surrounding the body, as shown in figure 8(*b*); this can also be seen in figure 8(*c*), where limiting streamlines show a one-signed tangential velocity. For $t \geqslant 7$, when the vortex–sphere distance is less than about 2.2, the boundary layer begins to depart from this equilibrium condition and its growth gradually accelerates. At time 8.5, when the filament distance has

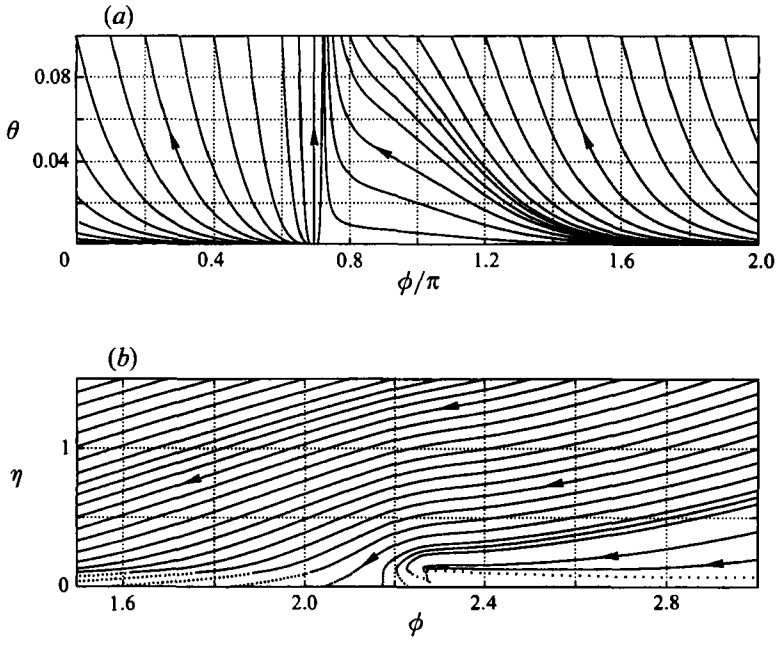

FIGURE 9. Vortex-induced boundary-layer development at $t = 8.5$, for initial vortex distance $d = 3$. (*a*) Limiting streamlines on the wall; (*b*) enlarged view of streamlines on the symmetry plane.

decreased to 1.92, the flow variations into the boundary layer have grown substantially. In figure 9(*a*), we can observe the limiting streamlines on the sphere surface at $t = 8.5$; no flow entering the symmetry plane is able to develop, as opposite to the preceding case, because of the well-established outflow annulus. An enlarged view of streamlines in the central region is shown in figure 9(*b*), on the (ϕ, η)-plane (the dotted lines indicate extrapolation of the streamline behaviour close to the wall after the last non-zero computed grid points). The pictures show the incipient formation of a stagnation point of attachment at $\phi = 2.16$; in this case, as opposed to the preceding one, we have a large outflow on the whole body surface which inhibits the formation of a separating stagnation point to close the local structure, and, looking at the whole of figure 9, we can catch a glimpse of a focus accompanied by outflow at $\phi = 2.30 \approx 0.73\pi$, attached to the wall. The structure given by a focus enclosed between two stagnation points, as observed in the case of $d = 1$, is not able to develop completely here because of the outflow, which inhibits the separating stagnation point and maintains the focus very close to the surface. In any case this deformed three-dimensional local structure is able to grow, pushing the field of secondary vorticity, increasing the spatial gradients, until at $t = 8.9$ the numerical discretization becomes inadequate to follow such variations and the model fails to converge.

6. Critical-point reconstruction

It is often of particular interest to understand the flow field close to a rigid boundary, and in particular the characteristics of the most critical points. Following the approach presented by Perry & Fairlie (1974) (see also Perry & Chong 1986, 1987), we can expand the limiting velocity field, close to a no-slip boundary (this

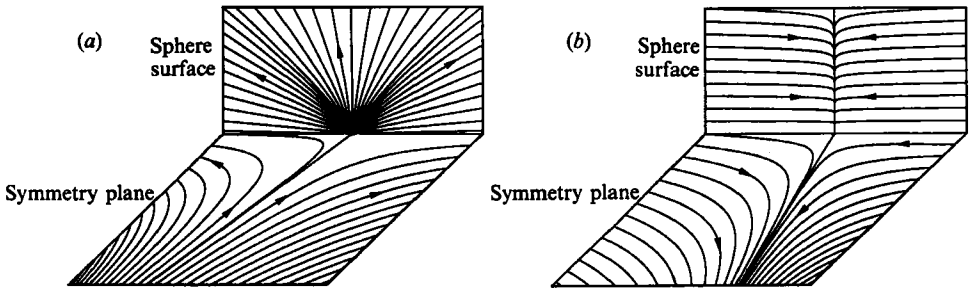

FIGURE 10. Reconstructed flow close to critical points in the boundary layer. Three-dimensional view at $t = 0.225$, for initial vortex distance $d = 1$. Limiting streamlines are shown on the sphere surface and on the symmetry plane. (*a*) Critical point P1 at $\phi = 2.39$; (*b*) critical point P2 at $\phi = 2.87$.

means mathematically that the limit $\tilde{y} \to 0$ is assumed) in a first-order Taylor series around a critical point, this gives

$$u_i/x_2 = B_{ij} x_j; \tag{33}$$

where, in our notation, $\boldsymbol{u} = [u, w, v]'$ and $\boldsymbol{x} = [\phi, \tilde{y}, \theta]'$.

In the present situation, the motion is on the $(\phi, \tilde{y})$-plane, so that the matrix $\boldsymbol{B}$ takes the simpler structure

$$\boldsymbol{B} = \begin{bmatrix} a & b & 0 \\ c & d & 0 \\ 0 & 0 & B_{33} \end{bmatrix}. \tag{34}$$

One eigenvector of the matrix is directed as θ, and the eigenspace described by the other two eigenvectors is the symmetry plane (or contained in it). The classification of the critical points is given by the analysis of the flow on the symmetry plane, i.e. the minor B_{22}, and in particular by it trace, $p = -(a+d)$, and its determinant, $q = ad - bc$. In this formulation the five unknown coefficients of the matrix $\boldsymbol{B}$ can be estimated by the first derivatives of the velocity field close to the surface.

In the case of $d = 1$ at time $t = 0.225$ we can recognize two critical points on the surface, say P1 and P2, at $\phi = 2.39$ and $\phi = 2.87$ respectively. For P1 we get $p = -0.55$ and $q = -113.13$, classifying P1 as an entering saddle, for P2 we get $p = 34.06$ and $q = -2083.10$, an exiting saddle. The reconstructed three-dimensional fields are reported in figures 10(*a*) and 10(*b*) for the points P1 and P2 respectively. We can observe the full three-dimensional structure of the point P1, as expected, since the value of B_{33} is comparable with the terms in the minor B_{22}, due to its localization in a region of strong outflow, as observed in §5. On the other hand the value of B_{33} for P2 is one order of magnitude smaller than the other terms in the matrix, and the flow is principally two-dimensional with a very small inflow from the third dimension.

In the second case, when $d = 3$, the situation is slightly different because of the presence of outflow along the entire boundary annulus. We looked at time $t = 8.5$, and recognized a critical point, say P3, at $\phi = 2.16$, and another less definite one, P4, at $\phi = 2.30$. In this case the smallness of the flow structure near the wall with the low spatial resolution suggest interpreting this reconstruction only in the sense of a glimpse, or suggestion, of the qualitative flow attached to the boundary. Computing the characteristics of P3 we get $p = 2$ and $q = -6.37$, this is again an entering saddle, whereas for P4 we obtain $p = 9.03$ and $q = 11.81$, classifying it is a stable focus. The two reconstructed flows are plotted in figures 11(*a*) and 11(*b*) respectively; we can

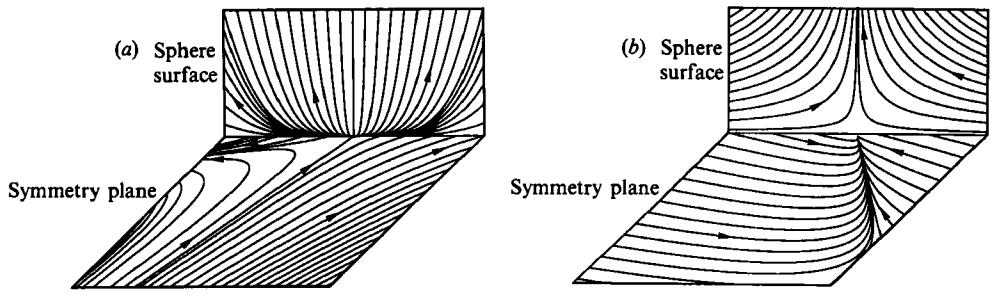

FIGURE 11. Reconstructed flow close to critical points in the boundary layer. Three-dimensional view at $t = 8.5$, for initial vortex distance $d = 3$. Limiting streamlines are reported on the sphere surface and on the symmetry plane. (*a*) Critical point at P3 $\phi = 2.16$; (*b*) critical point at P4 $\phi = 2.30$.

observe that P3 is a very distorted saddle, influenced by the other close critical point. In figure 11 (*b*) we can clearly recognize the three-dimensional focus attached to the wall.

7. Conclusion

In this work the close interaction of an infinitely long vortex filament and a rigid sphere is analysed at very high Reynolds number. No general method exists to simulate high-Reynolds-number flows and different models have to be used separately in order to study different features of such flow fields. However, care must be taken and the range of validity of the model employed must be stated.

First, the close interaction has been described assuming that the fluid is inviscid. The calculation has been performed using the classical cutoff method, and the initial conditions have been taken when the vortex filament is at a distance from the sphere equal to the radius R. The vortex filament approaches the surface of the sphere and stretches along it creating two opposite symmetrical kinks, which eventually touch each other to give rise to a highly stretched vortex ring, which lies almost on a meridian plane.

The cutoff model is unable to describe the reattachment between the two parts of the vortex filament and must be abandoned, but the vortex singularity model can be employed, since it includes an intrinsic numerical viscosity able to account for the viscous effect dominant in the lengthscale of the vortex filament core and dominant in the reattachment process. The results of the calculation are quite different from the previous case and the weak viscous effect causes the splitting of the filament when the vortex core touches the surface of the body and the consequent reconnection with the vortex image inside the sphere. Therefore no vortex ring is generated.

However in real fluids when solid boundaries are present a no-slip velocity condition exists, which prohibits vortex tubes from closing at the wall, and an unsteady boundary layer, due to the flow induced at the wall by the vortex filament, is expected to grow and interact with the inviscid external flow field. A timescale analysis has shown that the growth of the boundary layer is faster than the inviscid looping, which is faster than the reattachment process. Therefore the boundary-layer evolution, as induced by the fully inviscid external flow field, has been calculated by a method which allows the computation of the three-dimensional boundary-layer approximation close to the symmetry plane.

First the unsteady boundary layer has been analysed when the evolution of the vortex filament starts at a distance equal to the sphere radius. It rapidly grows into an internal secondary vortical structure, which may interact with the primary vortex of opposite circulation, and induces a recirculation region attached at the wall. This recirculation region is contained, at the wall, between two stagnation points, respectively of attachment and of separation, and resembles the separation observed in a two-dimensional vortex-driven boundary layer, with the main difference being that the streamlines, in the separated region, do not form closed loops but spiral into a focus. This is due to the presence of a flow leaving the symmetry plane, which is established close to the wall everywhere but in a small portion of relatively weak inflow. The presence of this inflow permits the presence of the separating stagnation point.

Secondly, the starting position of the vortex filament has been taken at a larger distance from the body. The boundary-layer evolution is shown to be dependent on the initial distance between vortex filament and body surface. In fact, until the filament approaches the sphere within a distance comparable with the sphere diameter, the timescale of the flow induced by the vortex is larger than that of the boundary layer, therefore the flow field at the wall has time to adjust to a stable, quasi-steady, boundary-layer configuration. The major feature is flow leaving the symmetry plane, from a annulus surrounding the body. This three-dimensional effect makes the appearance of a separating stagnation point difficult, and leads to a separation which seems not to produce the recirculation region at the wall. This behaviour of the three-dimensional flow field has been analysed by means of a critical-point approach.

The boundary-layer calculations suggest, in both cases, that eventually a final separation, along with the generation of a secondary vortex structure ejected far from the wall, may happen. Therefore we should expect a pairing process between the secondary and the primary vortices of opposite circulation, leading to the rebounding of the approaching vortex filament. The approximated modelling of the boundary layer certainly hides some features of the three-dimensional development of the flow field at the wall, and so here the fully viscous–inviscid interaction could not be properly reproduced.

This work has been supported by MURST-40%. The author is grateful to Prof. Bernardo De Bernardinis for his scientific advice during the research work.

REFERENCES

AGISHTEIN, M. E. & MIGDAL, A. A. 1986 Computer simulation of three-dimensional vortex dynamics. *Mod. Phys. Lett.* A **1**, 221.

AKSMAN, M. J. & NOVIKOV, E. A. 1988 Reconnection of vortex filaments. *Fluid Dyn. Res.* **3**, 239.

AKSMAN, M. J., NOVIKOV, E. A. & ORSZAG, S. A. 1985 Vorton method in three-dimensional hydrodynamics. *Phys. Rev. Lett.* **54**, 2410.

BATCHELOR, G. K. 1967 *An Introduction to Fluid Dynamics.* Cambridge University Press.

BLONDEAUX, P. & DE BERNARDINIS, B. 1983 On the formation of vortex pairs near orifices. *J. Fluid Mech.* **135**, 111.

CHORIN, A. J. 1982 The evolution of a turbulent vortex. *Commun. Math. Phys.* **83**, 517.

DHANAK, M. R. 1981 Interaction between a vortex filament and an approaching rigid sphere. *J. Fluid Mech.* **110**, 129.

DHANAK, M. R. & DE BERNARDINIS, B. 1981 The evolution of an elliptic vortex ring. *J. Fluid Mech.* **109**, 189.

DOLIGALSKI, T. L. & WALKER, J. D. A. 1984 The boundary layer due to a convected two-dimensional vortex. *J. Fluid Mech.* **139**, 1.

ERSOY, S. & WALKER, J. D. A. 1987 The boundary layer due to a three-dimensional vortex loop. *J. Fluid Mech.* **185**, 569.

HARVEY, J. K. & PERRY, F. J. 1971 Flowfield produced by trailing vortices in the vicinity of the ground. *AIAA J.* **9**, 1659.

LIGHTHILL, M. J. 1956 The image system of a vortex element in a rigid sphere. *Proc. Camb. Phil. Soc.* **52**, 317.

MEIRON, D. I., SHELLEY, M. J., ASHURST, W. T. & ORSZAG, S. A. 1988 Numerical studies of vortex reconnection. In *Proc. SIAM Workshop on Vortex Dynamics, April 25–27, Leesburg, VA.*

MOORE, D. W. 1972 Finite amplitude waves on aircraft trailing vortices. *Aeronaut. Q.* **23**, 307.

MOORE, D. W. & SAFFMAN, P. G. 1972 The motion of a vortex with axial flow. *Phil. Trans. R. Soc. Lond.* A **272**, 403.

NOVIKOV, E. A. 1983 Generalized dynamics of three-dimensional vortical singularities (vortons). *Sov. Phys. JETP* **57**, 566.

PEACE, A. J. & RILEY, N. 1983 A viscous vortex pair in ground effect. *J. Fluid Mech.* **129**, 409.

PEDLOSKY, J. 1979 *Geophysical Fluid Dynamics.* Springer.

PEDRIZZETTI, G. 1991*a* Stretching of a vortex filament over an approaching sphere using the vortex singularities method. *DIC* I-3. Università di Firenze.

PEDRIZZETTI, G. 1991*b* About modelling the close interaction between a vortex filament and a rigid sphere. Paper presented at *EUROMECH 1st EFMC, September 16–20, Cambridge University.*

PEDRIZZETTI, G. 1992 Insight to singular vortex flows. *Fluid Dyn. Res.* (in the press).

PERIDIER, V. J., SMITH, F. T. & WALKER, J. D. A. 1991 Vortex-induced boundary layer separation. Part 1. The unsteady limit problem $Re \to \infty$. *J. Fluid Mech.* **232**, 99.

PERRY, A. E. & CHONG, M. S. 1986 A series-expansion study of the Navier–Stokes equations with application to the three-dimensional separation pattern. *J. Fluid Mech.* **173**, 207.

PERRY, A. E. & CHONG, M. S. 1987 A description of eddying motion and flow pattern using critical-point concepts. *Ann. Rev. Fluid Mech.* **19**, 125.

PERRY, A. E. & FAIRLIE, B. D. 1974 Critical points in flow patterns. *Adv. Geophys.* **18B**, 299.

PUMIR, A. & SIGGIA, E. D. 1987 Vortex dynamics and the existence of solutions to the Navier–Stokes equations. *Phys. Fluids* **30**, 1606.

SAFFMAN, P. G. 1980 *Transition and Turbulence* (ed. R. E. Meyer), p. 149. Academic.

SAFFMAN, P. G. 1989 A model of vortex reconnection. *J. Fluid Mech.* **112**, 395.

SIGGIA, E. D. 1985 Collapse and amplification of a vortex filament. *Phys. Fluids* **28**, 794.

SMITH, C. R., WALKER, J. D. A., HAIDAIR, A. H. & SOBRUN, U. 1991 On the dynamics of near-wall turbulence. *Phil. Trans. R. Soc. Lond.* A **336**, 131.

VAN DOMMELEN, L. L. 1990 On the Lagrangian description of unsteady boundary-layer separation. Part 2. The spinning sphere. *J. Fluid Mech.* **210**, 627.

VAN DOMMELEN, L. L. & COWLEY, S. J. 1990 On the Lagrangian description of unsteady boundary-layer separation. Part 1. General theory. *J. Fluid Mech.* **210**, 593.

WALKER, J. D. A. 1978 The boundary layer due to a rectilinear vortex. *Proc. R. Soc. Lond.* A **359**, 167.

WALKER, J. D. A., SMITH, C. R., CERRA, T. & DOLIGALSKI, T. L. 1987 The impact of a vortex ring on a wall. *J. Fluid Mech.* **181**, 99.

WINCKELMANS, G. & LEONARD, A. 1988 Improved vortex methods for three-dimensional flows. In *Proc. SIAM Workshop on Vortex Dynamics, April 25–27, Leesburg, VA.*